Evaluation of stress corrosion cracking of irradiated 304L stainless steel in PWR environment using heavy ion irradiation

Jyoti Gupta, Jérémy Hure, Benoit Tanguy, Lydia Laffont-Dantras, Marie-Christine Lafont, Eric Andrieu

Evaluation of stress corrosion cracking of irradiated 304L stainless steel in PWR environment using heavy ion irradiation

J. Gupta [a, b], J. Hure [a], B. Tanguy [a, *], L. Laffont [b], M.-C. Lafont [b], E. Andrieu [b]

[a] CEA Saclay Université de Paris-Saclay, DEN, Services d'Etudes des Matériaux Irradiés, 91191 Gif-sur-Yvette Cedex, France
[b] Institut CARNOT, CIRIMAT-ENSIACET, 4 allée Emile Monso, 31030 Toulouse Cedex 4, France

A B S T R A C T

IASCC has been a major concern regarding the structural and functional integrity of core internals of PWR's, especially baffle-to-former bolts. Despite numerous studies over the past few decades, additional evaluation of the parameters influencing IASCC is still needed for an accurate understanding and modeling of this phenomenon. In this study, Fe irradiation at 450 °C was used to study the cracking susceptibility of 304 L austenitic stainless steel. After 10 MeV Fe irradiation to 5 dpa, irradiation-induced damage in the microstructure was characterized and quantified along with nano-hardness measurements. After 4% plastic strain in a PWR environment, quantitative information on the degree of strain localization, as determined by slip-line spacing, was obtained using SEM. Fe-irradiated material strained to 4% in a PWR environment exhibited crack initiation sites that were similar to those that occur in neutron- and proton-irradiated materials, which suggests that Fe irradiation may be a representative means for studying IASCC susceptibility. Fe-irradiated material subjected to 4% plastic strain in an inert argon environment did not exhibit any cracking, which suggests that localized deformation is not in itself sufficient for initiating cracking for the irradiation conditions used in this study.

1. Introduction

Austenitic stainless steel, owing to its high strength, ductility, and fracture toughness, has been selected as the structure alloy for the majority of the core internals of the Pressurized Water Reactor (PWR). However, the core internal components made of stainless steels have been shown to experience Irradiation Assisted Stress Corrosion Cracking (IASCC), which may affect the integrity of the PWRs. Core internals are in close proximity to the core and face significant neutron irradiation of up to 80 dpa during the designed lifetime of a PWR. This irradiation damage has a devastating influence on the material as it modifies the microstructure (by inducing defects such as dislocation loops, precipitates, cavities, etc.) and consequently the mechanical properties (such as tensile properties, ductility, and fracture toughness) [1–4]. The complex coupling of various parameters, as a consequence, complicates the identification of a comprehensive mechanism responsible for IASCC. Indeed, it has been suggested that various factors contribute to IASCC, and efforts should be made to account for the most significant factors [5].

Several factors such as Radiation Induced Segregation (RIS), radiation hardening, oxidation, and radiolysis have been proposed as likely contributors to IASCC. The role of Cr depletion, which has long been believed to be a detrimental contributor to IASCC in oxidizing environments, has been called into question in a PWR environment [6]. Post-irradiation annealing of ion-irradiated grades of 304 stainless steel has been shown to lead to a strong mitigation of IASCC, although virtually no RIS altering was observed [7]. The role of strain localization in plastically strained neutron-irradiated stainless steels at high temperature (~300 °C) has been highlighted as a potential primary contributor to IASCC [8,9]. The interaction of dislocation channels or strained-induced twins with the grain boundaries could be a source of high local strain and stress concentration at the boundaries, which could subsequently lead to the cracking of these boundaries. Several studies dealing with neutron irradiation [9–12] have reported a strong correlation between dislocation channels interaction with grain boundary and grain boundary fracture, even in an inert argon environment. Studies have also shown, on the contrary, that localized deformation cannot lead to intergranular fracture in a low electro-chemical

* Corresponding author.
E-mail address: benoit.tanguy@cea.fr (B. Tanguy).

http://dx.doi.org/10.1016/j.jnucmat.2016.04.003

potential (ECP) aqueous environment [13]. These conflicting results suggest that the role of localized deformation in initiating intergranular cracks in irradiated materials during straining is still not clear, and therefore, more work needs to be done in this direction.

As working with neutron irradiated material is quite difficult and expensive, emulation of neutron defect structures using different types of ion irradiations (H^+, Ni^{2+}, Xe^{26+}, Fe^{n+}) has been performed in several studies [14–23]. Proton irradiation is one of the most common methods. Being lighter and of moderate energy (several MeV), protons have a range of tens of microns in the material (typically the order of the grain size). As a consequence, proton irradiation has been proven to be a highly valuable tool to mimic irradiation effects in LWR's, i.e. RIS, irradiated microstructure, radiation hardening, and IASCC susceptibility [14,16]. The similarity of the deformation modes observed in neutron- and proton-irradiated stainless steels [10,16] has further promoted the use of proton irradiation as a surrogate to investigate the detrimental effect of localized deformation on intergranular cracking. Quantitative [16] and qualitative [17] investigations on the degree of strain localization (determined by slip-line spacing and step height measurements) induced by proton irradiation in stainless steel have been performed in an inert environment. These studies have shown that dislocation channeling becomes the major deformation mode at doses higher than a few dpa, depending on the SFE of the alloy. It is well known that low stacking fault energy (SFE) promotes planar slip [24] and hence, a higher degree of localization in irradiated material [5]. The degree of localized deformation, as represented by either the density of steps or by their spacing on grain surface or in a quantitative manner by the average height of steps, was shown to increase with dose [16,17] as well. This increase in the degree of localized deformation with dose was initially correlated with the increase of intergranular cracking with dose, as reported in Ref. [10]. Further evidence for this correlation between the degree of localized deformation (as measured by the weighted average height of slip-lines), and the cracking susceptibility (as measured by the crack length per unit area) was reported in Ref. [18] based on Slow Strain Rate tensile (SSRT) tests in a BWR environment. In addition, this study proposed that a certain amount of localized deformation is necessary to obtain Inter-Granular Stress Corrosion Cracking (IGSCC), which is related to the surface oxide film breakage either by grain boundary sliding [17] or by the high local stresses induced locally by dislocation channel-grain boundary interactions [19].

Several studies have shown that proton irradiation is one of the best available tools to replicate neutron irradiation damage, but it has several limitations. For example, the damage rate for proton irradiation ($\sim 10^{-6} - 10^{-5}$ dpa/s) is lower in comparison to heavy ion irradiation ($\sim 10^{-4} - 10^{-3}$ dpa/s), making the former more time consuming and hence less favorable to attain higher damage rates.

Heavy ion irradiation (for example, using Ni and Fe) can also produce irradiation induced defects (e.g. Frank loops) and a deformation microstructure similar to those one observed in neutron-irradiated stainless steels [20,21]. Yet heavy ion irradiation has been criticized due to the small penetration depths of heavy ions in material. Small penetration depths could alter the deformation structure at the surface, which could greatly affect IASCC tests, especially if strain localization is the main contributing factor. The relation between penetration depth and strain localization has recently been investigated [22]. It was shown that the degree of localization (as measured by the average surface step height and spacing) after straining was alike for 1.2 MeV and 2 MeV H^+ irradiated material, while it was significantly lower for 2.8 MeV Fe^{2+} irradiated material. This led to the conclusion that if the irradiation depth is greater than 1/3 of the average grain size, the average surface step height and spacing are weakly affected. Nevertheless, a successful use of 6 MeV Xe^{26+} ion irradiation to study IASCC sensitivity in Z6CND17.12 austenitic stainless steel (close to AISI 316) was demonstrated in Ref. [23]. With this heavy ion, an irradiation damage depth of 0.8 μm was obtained. Although the irradiation damage depth was much smaller than the grain size, an increase of IASCC sensitivity with increasing dose was reported in this study. However, the martensitic phase transformation Fe–γ → Fe–α resulting from the irradiation was potentially involved in cracking, so a direct and clear link with localization of deformation could not be drawn. There is currently a need to study the mechanisms of IASCC and the contribution of localized deformation in intergranular cracking of austenitic stainless steels in PWR environment using heavy ion irradiation. Heavy ions allow higher doses to be obtained faster than with protons, but they induce a significantly lower degree of localization. Hence, their use to study IASCC susceptibility appears to be an important milestone.

The objective of this study is to determine if heavy-ion irradiation with shallow damage depth can be an efficient tool to study the IASCC phenomenon. In this study, Constant Extension Rate Tensile (CERT) tests were conducted in a simulated PWR primary water environment on 10 MeV Fe^{5+} irradiated SA 304L (with an irradiation depth of about 2 μm) to study the relation between slip-line spacing and cracking susceptibility of the material.

2. Experimental techniques

2.1. Material and irradiations conditions

The material used in this study is commercial grade AISI 304L stainless steel. The chemical composition is Fe – 18.75Cr – 8.55Ni – 0.02Mo – 0.45Si – 1.65Mn – 0.012C–0.01P – 0.002S (wt %). The stacking fault energy of the material calculated using Pickering's formula is 23 mJ/m^2 [25]. The material was solution annealed at 1050 °C for 30 min followed by quenching with helium. The mean grain size was 27 μm. Tensile specimens with gauge sections of length 18.0 mm, width 2.0 mm, thickness 2.0 mm, and overall length of 40.0 mm were fabricated along with bars of cross section 2 mm × 2 mm and length 18 mm using electro spark technique. Tensile samples were used to perform mechanical tests, while bars were used to characterize the irradiated microstructure.

Prior to irradiation, these samples were mechanically polished back and front using ¼ μm diamond paste followed by vibratory polishing (on the face to be irradiated) in OPS solution for 10 h to eliminate surface hardened zones induced by mechanical polishing. Irradiation experiments were conducted using 10 MeV Fe^{5+} ions in an electrostatic accelerator connected to a triple beam chamber at the JANNuS facility of CEA Saclay [26]. Tensile specimens and bars were irradiated simultaneously to 5 dpa K–P at 450 °C with a dose rate of 2.7×10^{-4} dpa/s (calculated at the surface). A higher irradiation temperature (450 °C) was used in order to compensate for the effect of higher dose rate ($\sim 10^{-4}$ dpa/s for ion in comparison to 10^{-8} dpa/s for neutron) on microstructural evolution associated with ion irradiation. A temperature shift of 110 °C was calculated using temperature shift formulas available in the literature [5]. These formulas indicated that to obtain a microstructure similar to neutron irradiation at 340 °C using Fe irradiation, irradiation needs to be conducted at a temperature of 370 °C, while for similar microchemistry (RIS), an irradiation temperature of 550 °C is required [5]. Hence, an irradiation temperature of 450 °C was used in this study as a compromise between the two parameters. Besides, several studies [20] have previously conducted heavy ion irradiations at 450–500 °C to obtain irradiation induced microstructures and RIS close to that obtained with neutron irradiation at 340 °C, which further justifies the choice of a 450 °C irradiation temperature.

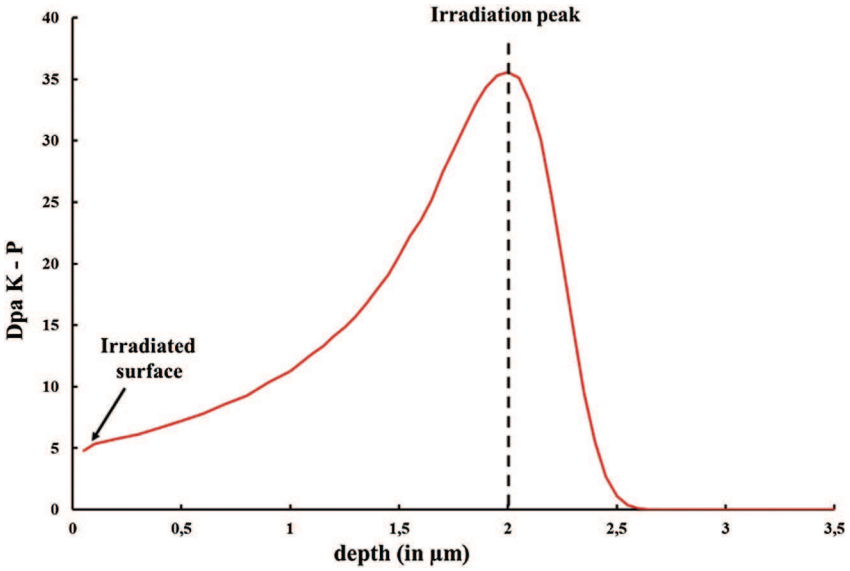

Fig. 1. Irradiation damage profile for 304L irradiated with 10 MeV Fe^{5+}. Damage was calculated with K–P approximation and plotted as a function of irradiation depth. Damage at the irradiated surface will be used to indicate the damage in the sample.

During irradiation, the temperature was monitored by a two-dimensional thermal imager (FLIR Type SC325) that monitored the temperature of the irradiated surface. The temperature was maintained to within ±20 °C of the set temperature. The penetration depth of 10 MeV Fe ions in the samples was about 2.5 μm. The damage profile obtained using SRIM-2011 with the Kinchin–Pease approximation and using a displacement energy of 40 eV is shown in Fig. 1 [27]. As recommended in Ref. [28], dpa K–P was used in this study. The damage will be cited as simply "dpa" from now on. Damage at the peak (35 dpa), located at a depth of 2 μm, is about 7 times the damage at the surface (5 dpa). Unlike the damage profile from protons, the damage profile for Fe irradiation does not have any constant damage (dpa) regions. So, the damage considered in this study will correspond to the damage at the surface i.e. 5 dpa, which is justified as most of the characterizations were performed at the surface. In addition, the irradiated zone in each sample was 10 mm × 2 mm, suggesting that all samples had both irradiated and unirradiated regions. This helped to have comparative studies in irradiated and unirradiated conditions independent of surface preparation.

2.2. Nanoindentation measurements

To assess the irradiation hardening, nanoindentation tests were incorporated. Nanoindentation measurements were performed at the Service de Recherche de Métallurgie Physique (SRMP) at CEA Saclay. For the tests, a Berkovich tip (three sided pyramid which is self-similar and has a half angle of 65°) with a radius of about 100 nm was used. A grid of 4 lines with 20 indents each was made corresponding to indent penetration depths of 2 μm, 1 μm, 500 nm and 250 nm. This grid has been used in order to assess the indentation size effect. The distance between two consecutive indents and between two lines was 40 μm. Indentations were performed in depth-control mode. The average of the 20 measured hardness values was considered for the each indent penetration depth. The duration of loading/unloading was fixed at 20s with the loading/unloading rate varying depending on the maximum load. A 5s hold time was used at the maximum load.

Measurements in both irradiated and unirradiated areas were made on the same surface of the bar in order to have an identical surface preparation. Moreover, indents in the unirradiated area were made 1.5 mm away from the irradiated-unirradiated transition zone[1] to avoid any interaction between the two regions.

2.3. Microstructure characterization

Transmission Electron Microscope (TEM) foils were prepared from 2 mm thick irradiated bars. The bars were mechanically ground to 80–120 μm and pre-thinned to near electron transparency using a dimple grinder from the unirradiated side. A Precision Ion Polishing System (PIPS) was used to make electron-transparent TEM foils. In this technique, two beams of Ar ions (5 keV each) were directed at an angle of 10° towards the center of the sample disc rotating at a speed of 3 rotations per minutes. TEM foils prepared using this approach were located close to the irradiated surface.

These foils were subsequently used to characterize the microstructure using a JEOL 2100 High Resolution Transmission Electron Microscope (HRTEM) operated at 200 kV available at UMS Castaing (Toulouse, France). Dislocation loops were examined using the long established Rel–Rod technique. In this technique, one of the four families of the Frank loops was highlighted by selecting the streak present in the diffraction pattern [29]. The presence of cavities was estimated using over and under focus technique. Images acquired in different perforation zones of several TEM foils were used to obtain a better statistic of each type of defect. The quantitative estimation (density and size) of these radiation-induced defects was performed on Dark Field TEM images using image analysis software. The software permitted the user to manually select the loops, and at the end of the analysis provided the mean density and size of the loops based on the selection made by user. To be transparent to electrons, the TEM foils should have thickness ranging between 70 and 150 nm. In this study a mean foil thickness

[1] The unirradiated area corresponds to the portion of sample which was under the metallic cover of the sample holder used during irradiation. As it was marked by metallic cover of the sample holder, irradiated – unirradiated transition zone was well defined.

of 100 nm has been taken to estimate the density of loops. This value is consistent with several others studies where similar materials have been characterized [30–32].

2.4. Constant extension rate tensile (CERT) testing

CERT tests were conducted in a tensile testing device CORMET C137 in the Service de Corrosion et du Comportement des Matériaux dans leur Environnement (SCCME) at CEA Saclay in a simulated PWR primary water chemistry environment. The setup consisted of an autoclave with a capacity of 5 L, a load frame, and a computer-driven 30 kN load train for straining the samples. The sample was mounted on heat-treated Inconel sample holder and into the load frame of the autoclave. The autoclave was filled with primary water (25–35 cc/kg H_2 STP, 1000 ppm B, 2 ppm Li), sealed, and pressurized with argon gas to detect any leakage. The temperature of the system was increased to reach the test temperature of 340 °C, and the pressure was maintained at 155 bars. Pressure and temperature were monitored using a PT (Pressure-Temperature) sensor located in the center of the autoclave. Prior to straining, environmental conditions were allowed to stabilize for a few hours. Pressure, dissolved oxygen content, and water conductivity were measured by sampling the water after the test. The displacements were measured by a Linear Variable Displacement Transducer (LVDT) located on the traction line of the autoclave. Load and displacement data was collected by a computerized data acquisition system and recorded every 10 s. After achieving stable conditions, the tensile specimen was strained at a rate of 5×10^{-8} s^{-1} up to 4% plastic strain.

One tensile test was conducted at 340 °C using the same tensile testing device in an argon environment to assess the cracking susceptibility of irradiated and unirradiated material in an inert environment.

2.5. Localized deformation and cracking characterization

After straining to a plastic strain of 4%, the spacing between slip-steps (as an indicator of deformation localization) and the number of cracks and crack length (as an indicator of cracking susceptibility) were estimated using SEM images of irradiated and unirradiated areas of the samples. SEM images were obtained using a FEI Helios 650 NanoLab Dual Beam FIB in SEM mode with an accelerating voltage of 5.0 kV and a working distance of 14 mm. The oxide layer on the sample after exposure to primary water was very thin, especially in the Fe irradiated area and hence, it did not obscure the visibility of step lines and cracks in the material. To investigate the nature of the crack, EBSD analysis was performed on thin samples prepared using a conventional FIB lift-out procedure using the same SEM. For this purpose, a location of interest was chosen and a layer of Platinum (Pt) was deposited on the sample. The coating was first made using electron beam and then using Gallium (Ga) ions beam to protect the area beneath from being contaminated by the Ga ions. Transverse cutting (i.e. in the direction perpendicular to the plane containing the crack) of the crack using large beam currents was then performed by milling two trenches on either side of the Pt coating. The sample of size 10 × 15 × 7 μm, was then mounted on a TEM sample holder and subsequently polished using successive low beam currents. Finally, the sample was thinned to 100 nm or less using 1 keV ion beam to minimize the artifacts from sample preparation and hence, to prepare a defect free surface for EBSD analysis. EBSD on this sample was then performed using a JEOL JSM 7001F Field Emission SEM at 30 kV in “in lens” mode. The mapping of the samples was done using a device on the JEOL microscope. The acquisition was done with Brucker software and post-treated with the HKL software.

3. Results and discussion

3.1. Microstructure

Heavy ion irradiation performed using 10 MeV Fe at 450 °C induced dislocation loops in the microstructure. Bright Field and Dark Field (g = ½ (3–11) on zone axis [011]) TEM images of the Frank loops are shown in Fig. 2. As is evident in the images, dislocation loops of different sizes were observed. For the majority of the loops, the diameter ranged between 6 and 14 nm. The largest loop size observed was 30 nm, while no loops smaller than 2 nm were identified. The size distribution of Frank loops is shown in Fig. 3. The size distribution appeared to be an asymmetric distribution that extended up to 30 nm, similar to what has been reported in literature for neutron-irradiated SS 304L [33]. The average number density and mean diameter of dislocation loops observed were $5 \pm 0.9 \times 10^{21}$ m^{-3} [2] and 13.4 ± 1.9 nm, respectively. The mean size of Frank loops obtained was similar to the value (12.5 nm) reported in Ref. [34] on 304 grade stainless steel irradiated with 2.8 MeV Fe at 300 °C at 10 dpa, and the number density was about a factor 10 lower in this study which may be due to the higher irradiation temperature, which tends to decrease the defect density as reported in Ref. [35]. No other irradiation-induced defects (e.g. cavities, radiation induced precipitates) were observed after 5 dpa in the studied material.

3.2. Irradiation hardening from nanoindentation measurements

Fig. 4 shows example load − displacement profiles obtained for different indents made at different depths (maximum depth of 2000 nm) in unirradiated samples. It can be seen from Fig. 4b that the reproducibility of the measurements was quite good. The evolution of the hardness as a function of the indentation depth for the unirradiated and irradiated samples is shown in Fig. 5a. The slight decrease in the measured hardness value with increasing indentation depth observed in unirradiated sample was attributed to the indentation size effect. In addition, in the irradiated sample, beyond a certain depth, the zone of plastic deformation originating from the indentation exceeds the boundary between the irradiated and unirradiated regions. As a consequence, a decrease in measured hardness was observed. At a 2 μm indentation depth, the contribution is entirely from the unirradiated region and hence, hardness values at this depth should be the same for the irradiated and unirradiated samples, as shown in Fig. 5a. To get rid of the indentation size effect, Nix and Gao have proposed a relation between the hardness at infinite depth (i.e. macroscopic hardness), H_0, and the measured hardness, H, at a given depth, D [36]. The square of the nanoindentation hardness is plotted against the reciprocal of indentation depth (1/D) in Fig. 5b for the unirradiated and irradiated samples. For the unirradiated sample a plot of the square of nanoindentation hardness is proportional versus the reciprocal of the indentation depth reveals excellent linearity. The bulk hardness, H_0 (square root of the intercept value), was estimated to be 2 ± 0.7 GPa for the unirradiated sample. The Vickers hardness value calculated from this bulk hardness value using the relation $H_v = 0.0945\ H_0$ was 191 ± 11 H_v [37,38]. Vickers hardness measurements performed on the unirradiated sample yielded a value of 200 ± 30 H_v which is in good agreement with the value reported above.

The depth of plastic deformation due to the indentation has also

[2] The average number density of Frank loops was obtained using a mean foil thickness of 100 nm. The error range is obtained by performing similar measurements on various images.

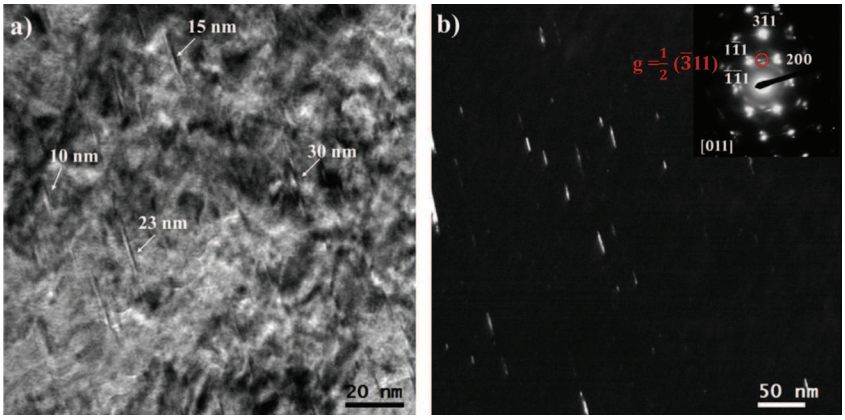

Fig. 2. a) Bright Field TEM image indicating the size of few Frank loops observed b) Rel-rod Dark Field TEM image obtained by selecting g = ½ (−311) streak (encircled in red) in the diffraction pattern (in inset) highlighting the Frank loops present in the microstructure of Fe irradiated 304L. (For interpretation of the references to color in this figure legend, the reader is referred to the web version of this article.)

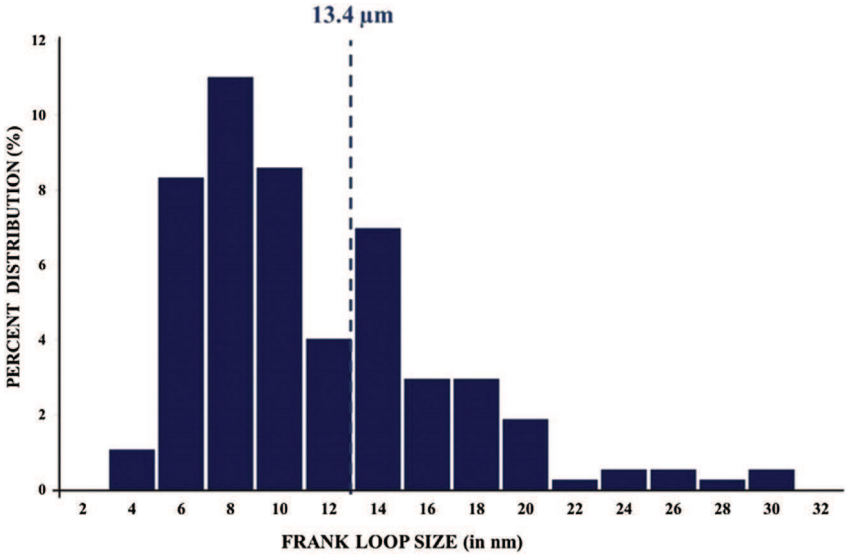

Fig. 3. Frank loops size distribution observed in Fe irradiated 304L to a dose of 5 dpa.

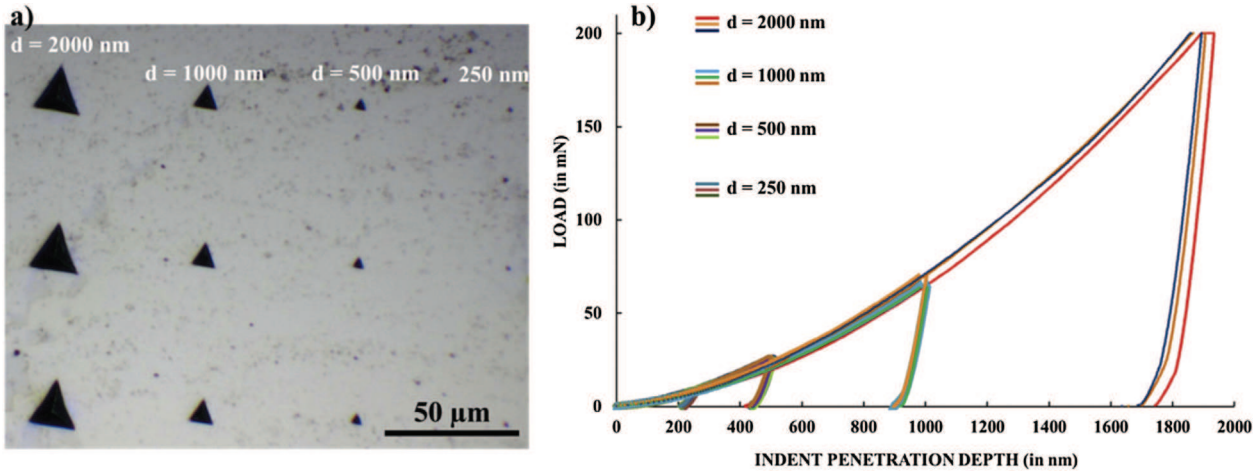

Fig. 4. a) Image of the nano indent matrix in the unirradiated region obtained using an optical microscope. b) Evolution of the load as a function of indent penetration depth during nanohardness indentation tests.

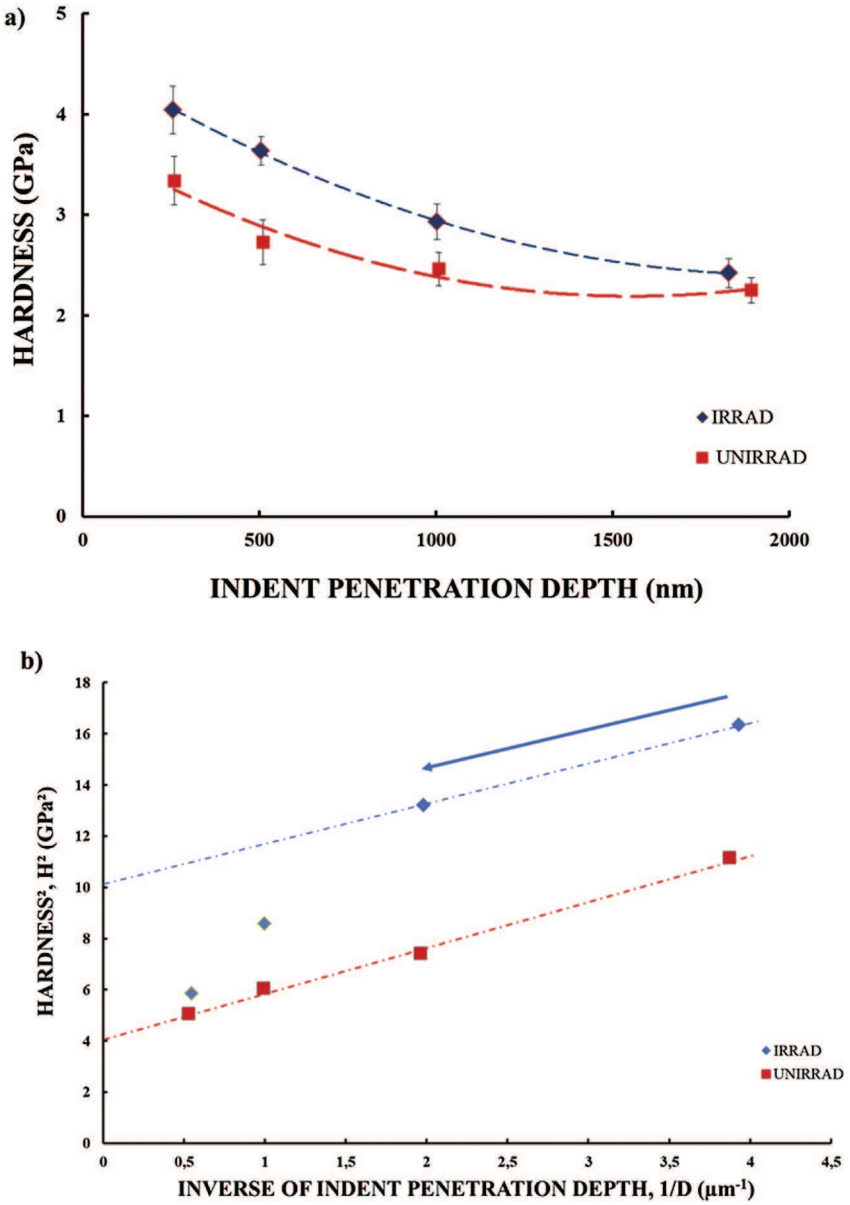

Fig. 5. Comparison of the a) hardness profiles b) Nix - Gao profile (H^2 versus 1/D) obtained for unirradiated and irradiated samples using nano indentation tests.

been shown to be dependent on the dose level [34]. The plastic deformation depth was estimated to reach 4 times the indentation depth for the 10 dpa Fe irradiated sample and up to 10 times the indentation depth for the unirradiated sample. Proceeding with this argument, an indentation depth of 500 nm in the irradiated sample will corresponds to a plastic zone extending to a depth of 2 μm. As the boundary between the irradiated and unirradiated regions is estimated to be at 2.5 μm, the hardness measured at 500 nm depth was considered unaffected by the unirradiated area. Assuming a linear relation, as was observed for unirradiated material, the bulk hardness for the irradiated material was evaluated using only the data from the inflexion points (1/D = 4 and 2) indicated with an arrow. In the irradiated sample, the square root of the intercept value was estimated to be 3.16 GPa. This suggests an increase of 1.16 GPa (or 58%) in the bulk hardness after irradiation. The dose that led to this increase in hardness was at least 5 dpa, as the irradiated region scanned via nano indentation presents a continuously varying damage ranging from 5 dpa to 35 dpa (see Fig. 1). However, it is known that the irradiation hardening of austenitic steel saturates at about 5–10 dpa, suggesting that the contribution of the damage close to the peak region or the surface region is not expected to be very different. Thus, it can be concluded that Fe irradiation at 450 °C to about 5 dpa leads to an irradiation hardening of ~58%. This hardening is linked to the defects (Frank loops) induced in the microstructure, which act as obstacles to the motion of dislocations.

3.3. Localized deformation

Plastic strain up to 4% at 340 °C produced fine lines representing surface offset in both the unirradiated and irradiated zones of the sample. Fig. 6 shows cartography obtained in the irradiated area using a ForeScattered Electron (FSE) imaging system of the e^- flash EBSD detectors. Due to its high sensitivity to small orientation

Fig. 6. EBSD cartography obtained using FSE after 4% plastic strain in the irradiated area.

irradiation. The probability density distribution of slip-line spacing given in Fig. 7 shows that the irradiation broadens the distribution towards larger values. An increase of slip-line spacing after ion irradiation has also been reported in Refs. [22,34] for 1.2 MeV H and 2.8 MeV Fe, respectively. Miura et al. [39] explained that the slip-step spacing widens due to blocking of some of the slips (present in an unirradiated matrix) by damage present in the irradiated region. The author further explained that the increase of step spacing means that the deformation is more localized in each slip. The spacing obtained after Fe irradiation in this study is significantly lower than that reported after proton irradiation (~9–10 µm for 2.5 dpa) of a SUS304 with a 30 µm grain size [22]. This is in accordance to the findings of Jiao and Miura and is attributed to the different penetration depths (or to be precise, the damage depth relative to the grain size) of the two ions in the material [22,39]. As the dislocation channel structure is linked to the localization of plasticity, larger spacing reflects a higher degree of localization [22].

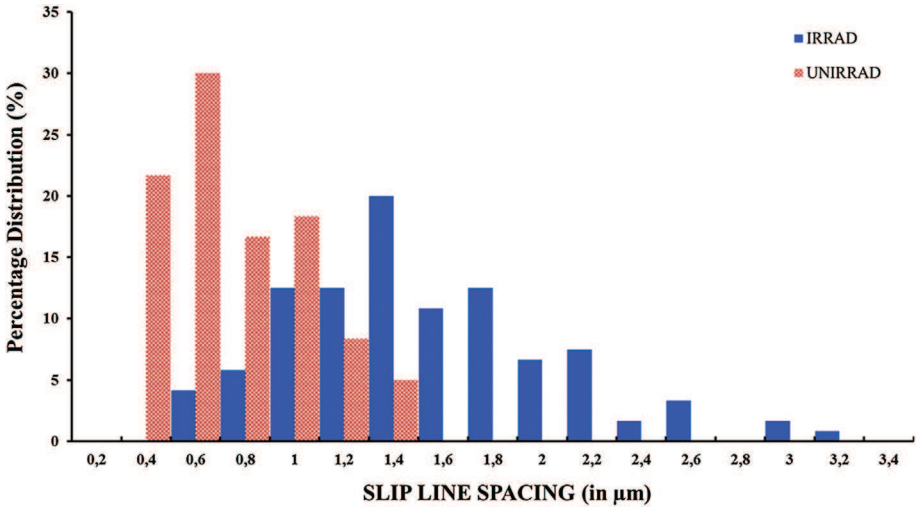

Fig. 7. Probability distribution of slip-line spacing measured in the unirradiated (in red) and Fe irradiated (in blue) region of the same sample after CERT up to 4% plastic deformation. (For interpretation of the references to color in this figure legend, the reader is referred to the web version of this article.)

changes, the cartography obtained using FSE included color contrast, which offered the opportunity to clearly see the grains. However, the information on the orientation, is qualitative, and colors cannot be related to a given orientation. Areas identified as ferrite phase are contoured in Fig. 6 using black dashed lines and constitute 4.7% of the total surface. Fine lines corresponding to slip-lines are clearly visible within austenite grains. It can be clearly seen that the number of lines per grain varies significantly from grain to grain, with some grains showing no lines at all. This variation of line number density within each grain is linked to the variation of grain orientation relative to the tensile loading direction and has been reported in previous studies [17].

The average slip-line spacing was computed over 10 SEM images (around 25 grains) for each condition. The value was 0.9 µm for the unirradiated zone[3] and 1.6 µm for the irradiated zone (Fig. 7) of the sample. This implies an increase of 77% in the slip-line spacing with

[3] This value has been shown to be reproducible based on several sets of measurements on approximately the same grain numbers (25 grains).

3.4. IASCC susceptibility

CERT tests were performed at 340 °C in a PWR environment in order to study the cracking susceptibility after irradiation. Since only a fraction of the gage length was irradiated (i.e. it had both unirradiated and irradiated regions), it gave an opportunity to study the impact of irradiation on cracking susceptibility of the material with the same environment, surface finish, and loading conditions. Inspection of the gauge length in both irradiated and unirradiated areas was performed using SEM. After 4% plastic strain, many cracks were observed on the irradiated area. An example of the surface observed in the irradiated area is shown in Fig. 8a. The intergranular nature of the cracks was clear from surface observations and was verified using transversely cut FIB samples. Fig. 8a illustrates an example of a random crack with a length of 60 µm in the irradiated area. The penetration depth of the crack was measured to be 2.2 µm (Fig. 8b), which seems to indicate that a crack arrest occurs in the vicinity of the boundary between irradiated and unirradiated material (recall that the depth of the irradiated area is ~2.5 µm, as indicated in Fig. 1). The crack initially

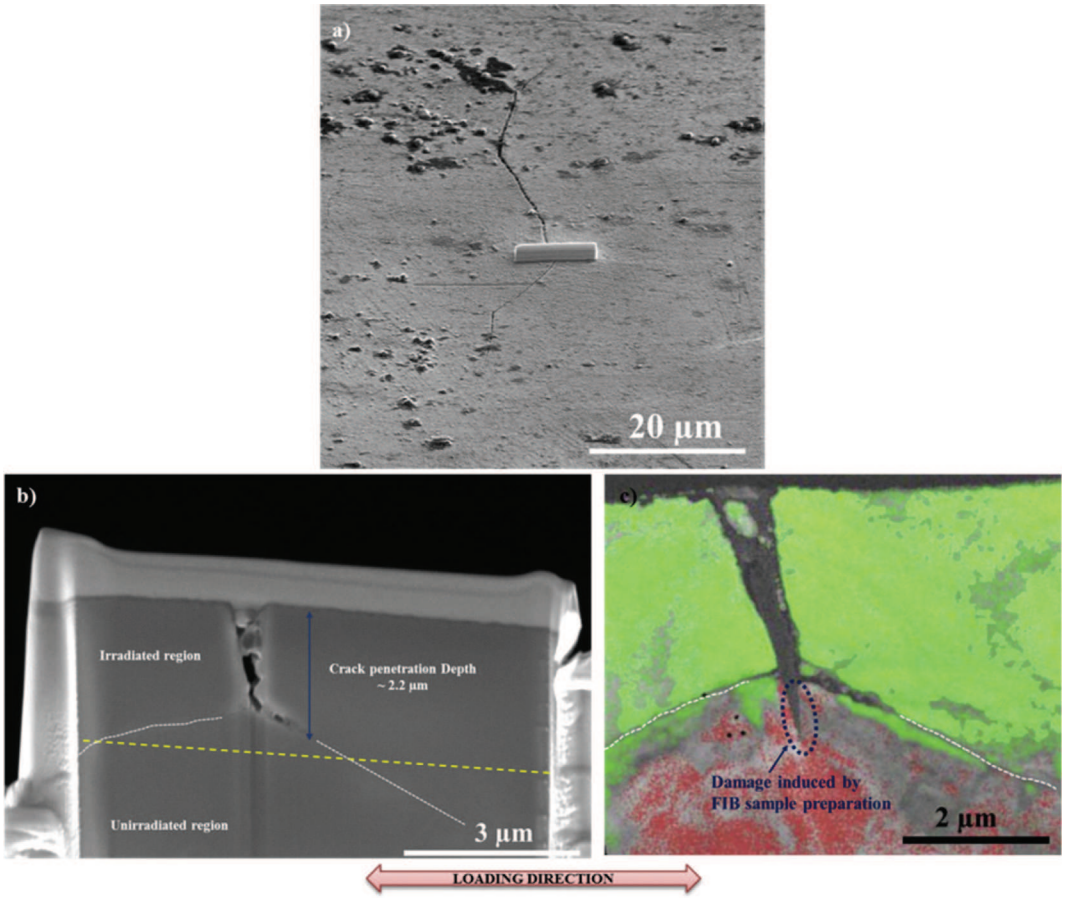

Fig. 8. a) SEM image of the crack cut using FIB b) zoomed cross-sectional image of the same crack after FIB cutting (yellow line marks the irradiated – unirradiated transition zone) c) Phase map (obtained using EBSD) of grains around cracks. Green represents austenite phase, while red corresponds to a Body Cubic Centered phase. Grain boundaries are marked in white dashed lines. (For interpretation of the references to color in this figure legend, the reader is referred to the web version of this article.)

propagated along the grain boundaries in a plane perpendicular to the loading direction and then changed direction. The branching of the crack was linked to the presence of a Body Cubic Centered (BCC) phase which was confirmed by EBSD analyses. Based on chemical analysis performed by TEM EDX, which shows that its chemical composition was similar to that of the austenite (different from ferrite), and from the quality patterns from EBSD, this BCC phase was inferred to be martensite. Complementary investigations on the origin of martensite phase are in progress. The grain boundaries cracked were of type RHAB (Randomly High Angle Boundaries) with angles ranging between 30° and 50°. This type of grain boundary has been identified to be strongly correlated with cracking [40].

Most of the cracks in the irradiated region were oriented perpendicular to the loading direction (Fig. 9a). A mean crack density of 302 cracks/mm^2 and mean crack length of 17 µm were determined. Surface steps are also clearly visible in this image. An identical experiment was conducted in inert Argon. Although slip-line features similar to those described above were observed (see Fig. 11d), no cracks were observed on this sample. The absence of cracks for this test emphasizes that for the irradiation conditions used in this study, a localized strain of 4% is not in itself sufficient for initiating intergranular cracking. In order for cracking to occur, grain boundaries must be embrittled, either by the corrosive environment or by RIS (Radiation Induced Segregation) induced by high irradiation doses or by the combination of two.

The crack length distribution is given in Fig. 10. Most of the cracks have lengths in the range 5–30 µm with a significant percentage (~45%) around 10 µm. A few cracks have a length up to 60 µm. The majority of the unirradiated area did not present any cracks, as shown in Fig. 9b. However, careful examination revealed the presence of a few small cracks in this region. Fig. 9b shows also that less surface slip-lines are apparently observed in the unirradiated region. This could be explained by the fact that for the same level of plastic strain, localization is less marked for the unirradiated area. Localization is linked to the height of the steps, so with a lower level of localization, less marked steps will be induced in this area.

Fig. 11 shows enlarged SEM images of different types of crack initiations. For most cases, the slip lines (i.e. surface steps) (represented by black dashed lines in Fig. 11) in a deformed grain were in a single direction, suggesting that one single slip system is dominant for these grains. Moreover, it is evident from the images that these slip-lines were present on either one or both sides of the cracked grain boundaries. Such slip-lines are commonly observed on irradiated stainless steels and have been reported to correspond to planar slip [9,16]. For a few grains, slip-lines were not visible. Open cracks are shown in Fig. 11a and b, where smaller cracks are indicated by white arrows. In Fig. 11a, slip-lines are visible on the two grains adjacent to the open crack. In this case, slip-lines clearly intersect the grain boundary where cracking has occurred. The role of slip-lines in grain boundary cracking is less clear in Fig. 11b,

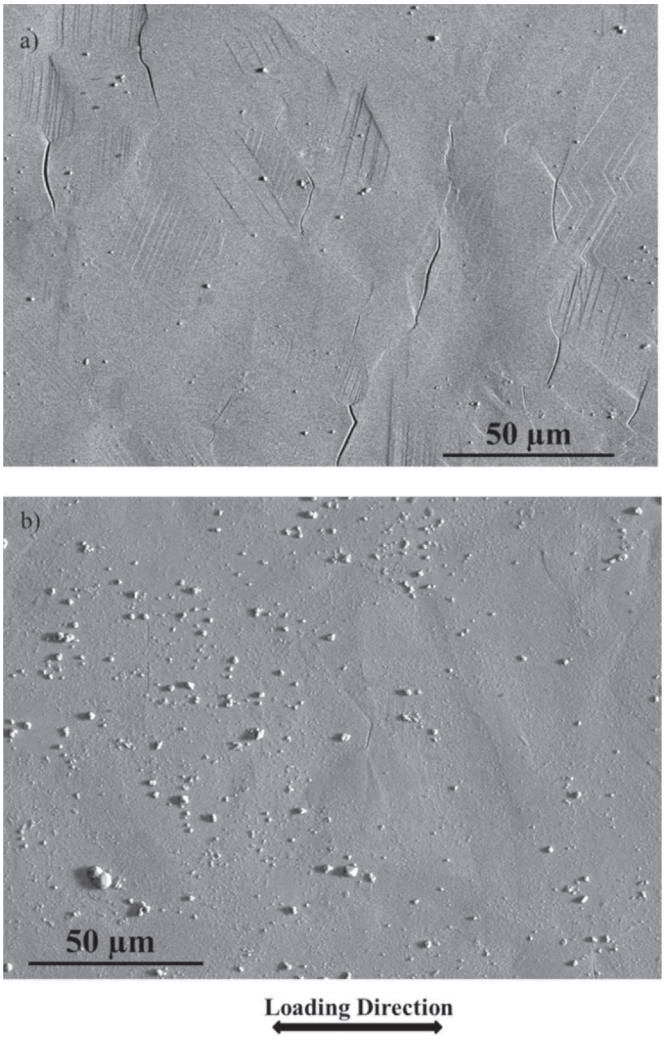

Fig. 9. Surface appearance of CERT specimens deformed up to 4% plastic strain in PWR environment as observed by SEM a) 5 dpa Fe b) unirradiated region. Loading direction is indicated below the images.

where slip lines are nearly parallel to the crack on one of the adjacent grains, but no slip-lines can be clearly identified in the second adjacent grain. Crack initiation as a result of the interaction of slip-lines with grain boundaries is clearly shown in Fig. 11c, where discontinuous slip between two adjacent grains is observed.

Quantitative characterization of crack initiation sites, as performed in Ref. [19], was not the aim of this study. However, morphologies of cracking similar to that seen in Fig. 11c have been reported in different studies devoted to IASCC cracking of plastically strained, irradiated stainless steel, either after neutron irradiation [9], or after proton irradiation [17,19,41]. The similarity in the morphologies of the cracks suggests the possibility of using Fe irradiation to study intergranular cracking susceptibility of the material.

4. Conclusions

This study assessed the stress corrosion cracking of 304L stainless steel irradiated with 10 MeV Fe^{5+} ions at 450 °C to 5 dpa and then plastically strained up to 4% in a simulated PWR water environment. The irradiation-induced microstructure, hardening, localization of plastic deformation (as measured by slip-lines spacing), and cracking were characterized based on TEM analyses, nano-indentation tests, CERT tests, and SEM analyses. The following results were obtained:

- For 5 dpa, the irradiation-induced microstructure consisted of Frank loops with density $5 \pm 0.9 \times 10^{21}$ m^{-3} and size 13.4 ± 1.9 nm.
- An increase of the bulk hardness of 56% after Fe irradiation was measured using nano-indentation tests. This increase is linked to the irradiation-induced microstructure.
- The Fe irradiated region presented a slip-line spacing that was 1.8 times greater than that of the unirradiated region of the sample. Despite a shallow irradiation depth (irradiation depth/grain size ~ 0.09), the increase in slip-line spacing suggests an increase in the degree of localization with Fe irradiation.
- Plastic strain of up to 4% in a PWR environment produced intergranular cracking of irradiated samples, suggesting an increase in susceptibility of the material with Fe irradiation. Crack

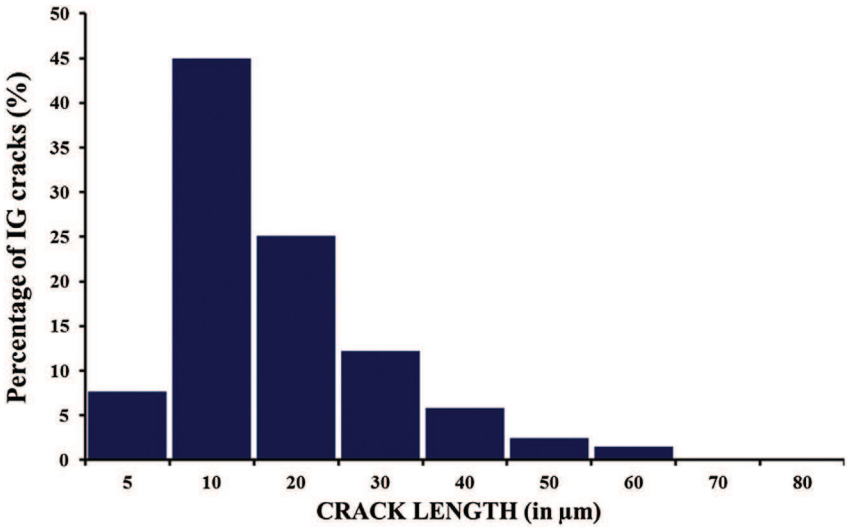

Fig. 10. Crack length distribution of 5 dpa Fe irradiated after 4% plastic strain.

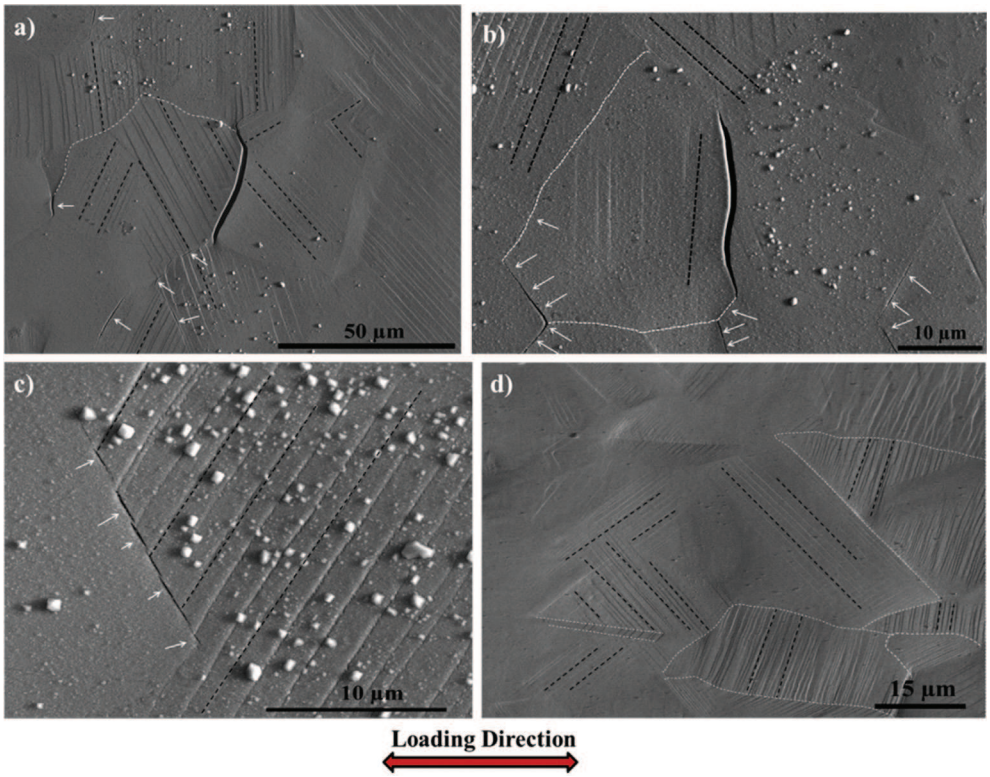

Fig. 11. Enlarged SEM images of cracks in Fe-irradiated stainless steel strained up to 4% plastic strain in a PWR environment (a, b, c) and of slip-lines (taken with a sample tilt of 52°) in Argon (d). Slip-lines direction within a grain are indicated by black dashed lines, small cracks are indicated by white arrows, several grain boundaries are indicated by white dotted lines.

initiation sites similar to those reported for neutron-irradiated or proton-irradiated stainless steels were observed.

- No cracks were observed in the Fe irradiated sample that was plastically strained in an inert environment, which indicates that for the irradiation conditions used in this study, localized strain is not in itself capable of initiating intergranular cracking.

Acknowledgment

The authors would like to thank Y. Serruys, E. Bordas and Team JANNuS (DMN/JANNUS, CEA Saclay) for their support and assistance in conducting the Fe irradiation. The authors would also like to acknowledge M. Rousseau (DPC/SCCME, CEA Saclay) for carrying out the mechanical tests, M. Jublot (DMN/SEMI, CEA Saclay) for his supervision during the FIB sessions and F. Barcelo (DMN/SRMA, CEA Saclay) for conducting the EBSD analysis.

References

[1] G.S. Was, P.L. Anderson, JOM 44 (1992) 8.
[2] S.M. Bruemmer, E.P. Simonen, P.M. Scott, P.L. Andersen, G.S. Was, J.L. Nelson, J. Nucl. Mater. 274 (1999) 299.
[3] C. Pokor, Y. Brechet, P. Dubuisson, J.P. Massoud, X. Averty, J. Nucl. Mater. 326 (2004) 30.
[4] O.K. Chopra, A.S. Rao, J. Nucl. Mater. 409 (2011) 235.
[5] G.S. Was, Fundamentals of Radiation Materials Science: Metals and Alloys, Springer, 2007.
[6] K. Fukuya, M. Nakano, K. Fujii, T. Torimaru, Y. Kitsunai, J. Nucl. Sci. Tech 41 (2004) 1218.
[7] J.T. Busby, G.S. Was, E.A. Kenik, J. Nucl. Mater. 302 (2002) 20.
[8] N. Hashimoto, S.J. Zinkle, A.F. Rowcliffe, J.P. Robertson, S. Jitsukama, J. Nucl. Mater. 283 – 287 (Part 1) (2000) 528.
[9] H. Nishioka, K. Fukuya, K. Fujii, Y. Kitsunai, J. Nucl. Sci. Tech 45 (2008) 274.
[10] C. Bailat, F. Groschel, M. Victoria, J. Nucl. Mater. 276 (2000) 283.
[11] K. Fukuya, M. Nakano, K. Fujii, T. Torimaru, J. Nucl. Sci. Tech 41 (2004) 673.
[12] T. Onchi, K. Dohi, N. Soneda, J.R. Cowan, R.J. Scowen, M.L. Castano, J. Nucl. Mater. 320 (2003) 194.
[13] H.M. Chung, R.V. Strain, W.J. Shack, Nucl. Eng. Des. 208 (2001) 221.
[14] G.S. Was, Z. Jiao, J.T. Busby, J. Nucl. Mater. 300 (2002) 198.
[15] K.J. Stephenson, G.S. Was, J. Nucl. Mater. 456 (2015) 85.
[16] Z. Jiao, J.T. Busby, G.S. Was, J. Nucl. Mater. 361 (2007) 218.
[17] Z. Jiao, G.S. Was, J. Nucl. Mater. 382 (2008) 203.
[18] Z. Jiao, G.S. Was, J. Nucl. Mater. 408 (2011) 246.
[19] M.D. McMurtrey, B. Cui, I. Robertson, D. Farkas, G.S. Was, Curr. Opin. Solid State Mater. Sci. 305 (2015) 305.
[20] J.I. Cole, S.M. Bruemmer, J. Nucl. Mater. 225 (1995) 53.
[21] A. Etienne, M. Hernandez-Mayoral, C. Genevois, B. Radiguet, P. Pareige, J. Nucl. Mater. 400 (2010) 56.
[22] Z. Jiao, J.G.S. Was, T. Miura, K. Fukuya, J. Nucl. Mater. 452 (2014) 328.
[23] R.-S. Wang, C.-L. Xu, X.-B. Liu, P. Huang, Y. Chen, J. Nucl. Mater. 457 (2015) 130.
[24] W. Karlsen, G. Diego, B. Devrient, J. Nucl. Mater. 406 (2010) 138.
[25] F.B. Pickering, Physical metallurgical development of stainless steels, in: Proceedings of the Conference on Stainless Steels 84, Gothenberg, Sweden, 1984, p. 2.
[26] L. Beck, Y. Serruys, S. Miro, P. Trocellier, E. Bordas, F. Leprêtre, D. Brimbal, T. Loussouarn, H. Martin, S. Vaubaillon, S. Pellegrino, D. Bachiller-Perea, J. Mater. Res. 30 (2015) 1183.
[27] ASTM Designation E 521-89, Annual Book of ASTM Standards, vol. 12.02, American Society for Testing and Materials, Philadelphia, PA, 1989, p. D-9.
[28] R.E. Stoller, M.B. Toloczko, G.S. Was, A.G. Certain, S. Dwaraknath, F.A. Garner, Nucl. Inst. Methods B 130 (2013) 75.
[29] A. Renault, J. Malaplate, C. Pokor, P. Gavoille, J. Nucl. Mater. 421 (2012) 124–131.
[30] A. Renault, C. Pokor, J. Garnier, J. Malaplate, in: Proceedings of 14th International Conference on Environmental Degradation of Materials in Nuclear Power Systems, Virginia, 2009, p. 1324.
[31] C. Pokor, Y. Brechet, P. Dubuisson, J.P. Massoud, X. Averty, J. Nucl. Mater. 326 (2004) 19.
[32] M. Millier, Ecole Nationale Supérieure des Mines de Saint Etienne [Phd thesis], 2014.
[33] D.J. Edward, E.P. Simonen, S.M. Bruemmer, J. Nucl. Mater. 317 (2003) 13.

[34] T. Miura, K. Fujii, H. Nishioka, K. Fukuya, J. Nucl. Mater. 442 (2013) 735.
[35] K. Kondou, A. Hasegawa, K. Abe, J. Nucl. Mater. 329 – 333 (Part A) (2004) 652.
[36] K. Yabuuchi, Y. Kuribayashi, S. Nogami, R. Kasada, A. Hasegawa, J. Nucl. Mater. 446 (2014) 142.
[37] W.D. Nix, H. Gao, J. Mech. Phys. Solid 46 (1998) 411.
[38] A. Lupinacci, K. Chen, Y. Li, M. Kunz, Z. Jiao, G.S. Was, M.D. Abad, A.M. Minor, P. Hosemann, J. Nucl. Mater. 458 (2015) 70.
[39] T. Miura, K. Fujii, K. Fukuya, Y. Ito, J. Nucl. Mater. 386–388 (2009) 210.
[40] M.D. McMurtrey, G.S. Was, L. Patrick, D. Farkas, Mater. Sci. Eng. A 528 (2011) 3730–3740.
[41] G.S. Was, F. Farkas, I.M. Robertson, J. Nucl. Mater. 300 (2002) 198;
(a) Curr. Opin. Solid State Mater. Sci. 16 (2015) 134.